β-γ angular correlations in ^{20}Na and ^{20}F beta decay

R. D. Rosa, W. W. Daehnick, Swapan K. Saha, and P. C. Li
Nuclear Physics Laboratory, University of Pittsburgh, Pittsburgh, Pennsylvania 15260
(Received 16 October 1987)

The β-γ angular correlations for the decay of ^{20}Na and ^{20}F to the 1.633 MeV state of ^{20}Ne have been measured using a twenty-detector system of cylindrical symmetry. ^{20}Na was produced by the ^{20}Ne(p,n)^{20}Na reaction using a 19 MeV proton beam, and ^{20}F was produced by the reaction ^{19}F(d,p)^{20}F using SF_6 gas and 4 MeV deuterons. The activated gasses were continuously transferred, through a thin capillary, from the target cell into the source cell in the center of the correlation apparatus. Two γ detectors and 16 β detector telescopes allowed for the simultaneous measurements of β-γ coincidences at 0°, 25°, 45°, 65°, 90°, 115°, 135°, 155°, and 180°, and at their symmetric counterparts with respect to the 0°–180° direction. The β-γ correlation was also measured for the first-forbidden β^- decay of ^{124}Sb, in order to confirm the computed attenuation in measured anisotropy caused by the finite geometry of the detectors and the source cell. The correlation function is denoted by $W_{\pm}(\theta_{\beta\text{-}\gamma})=1+\alpha_{\pm}(E)(p/E)^2\cos^2\theta_{\beta\text{-}\gamma}$. The $\pm$ subscripts refer to electron or positron decay, p is the beta momentum, and E is the beta total energy in MeV. The present result for ^{20}Na(β-γ) correlation is $\alpha_-(E)=(-4.45\pm0.31)\times10^{-3}E+(1.87\pm0.42)\times10^{-4}E^2$. The least squares fit to the energy dependence for ^{20}F was performed by assuming the quadratic energy dependence measured for ^{20}Na, and the linear term in $\alpha_+(E)$ yielded $\alpha_+(E)=(0.08\pm0.16)\times10^{-3}E$. First and second class induced pseudotensor form factors ($d_{\rm I}$ and $d_{\rm II}$) were evaluated by combining the linear energy dependences and yielded $d_{\rm II}/Ac=-1.1\pm0.7$ and $d_{\rm I}/Ac=11.3\pm0.7$. The 1977 Calaprice calculations for the value of the second-forbidden axial vector form factor j_2 were used. Assuming the Calaprice prediction for j_2, j_3 could be deduced from the quadratic term of the energy dependence of the asymmetry. We obtained $j_3=-(19.5\pm3.0)\times10^4$. We conclude that the angular correlations in mass 20 are close to and may be in agreement with expectations based on conserved vector current theory. Our best value for second class axial currents, $d_{\rm II}/Ac=-1.1\pm0.7$, is at the level of 10% of the weak magnetism term; however, the statistical error given and the large uncertainty in j_2, derived from shell model wave functions, preclude a more definite statement regarding the existence of second class currents.

I. INTRODUCTION

In the last decade, a number of experiments have been performed to measure induced weak currents in nuclear beta decay. At issue was the validity of the conserved vector current hypothesis (CVC),[1] which relates vector beta decay to the electromagnetic interaction, and the possible presence of G-parity nonconserving weak currents, known as second-class currents (SCC).[2] In order to measure these induced interactions, it is necessary to isolate them from the dominant allowed transitions, since they are quite small being recoil order corrections. In 1974 Holstein[3] showed that angular correlations in allowed beta decay are sensitive to recoil order corrections which destroy the first-order angular correlation isotropy of such decays. In particular, he showed that for a large enough energy release recoil order effects of order 2% are to be expected, provided that CVC is a good assumption, and provided that second-class currents do not significantly increase such asymmetries. The beta-gamma correlation for the mirror Gamow-Teller decays of the mass-20 system are particularly interesting in this respect, because of the relative simplicity of the decay schemes and the large energies released.

CVC can be deduced directly from unified gauge theories[4] of the weak and electromagnetic interactions. However, SCC contributions are difficult to explain in the unified theories proposed.[5] After some early results to the contrary, recent experiments which have been performed to test CVC and experiments sensitive to induced interactions are consistent with CVC and the absence of SCC. Confirmation of CVC provides a powerful way to analyze beta spectra, since via CVC all of the weak vector currents can be predicted from their analog electromagnetic processes. Therefore beta decay experiments can focus on determining the character of the axial vector interaction which has no electromagnetic analog.

In the Fermi theory of β decay the β-γ angular correlation of an allowed decay is isotropic, however, with inclusion of induced weak currents effects the angular correlation takes the form,[3]

$$W_{\pm}(\theta_{\beta\text{-}\gamma})=1+\alpha_{\pm}(E)(p/E)^2\cos^2\theta_{\beta\text{-}\gamma} \tag{1}$$

with

$$\alpha_{\pm}(E)\approx\frac{E}{4m_nAc}\left[1\pm b-(d_{\rm I}\pm d_{\rm II})-\frac{3}{2\sqrt{14}}\frac{j_2}{m_nA}(E_0-2E)-\frac{3}{\sqrt{35}}\frac{j_3}{m_nA}E\right]. \tag{2}$$

Hence $\alpha_{\pm}(E)$ can be written as a quadratic function in E:

$$\alpha_{\pm}(E)=B_{\pm}E+CE^2 , \tag{3}$$

where the $\pm$ alternation refers to electron or positron decay, E is the total beta energy, E_0 is the beta endpoint energy, p is the beta momentum, m_n is the nucleon mass, and A is the nuclear mass number. The other letters represent beta decay form factors that are commonly known as Gamow-Teller (c), weak magnetism (b), first-class induced tensor ($d_{\rm I}$), second-class induced tensor ($d_{\rm II}$), and second forbidden axial vector (j_2 and j_3) terms. The vector second forbidden contributions to $\alpha_{\pm}(E)$ are small and have been ignored in Eq. (2). The form factors can be related to single-particle nuclear matrix elements via the impulse approximation.[3]

From the ^{20}Na correlation alone, $d_{\rm I}$ and $d_{\rm II}$ cannot be evaluated independently. But ^{20}F and ^{20}Na correlations can be combined to separate b and $d_{\rm II}$ form factors from $d_{\rm I}$, j_2, and j_3. Subtracting $\alpha_-(E)$ from $\alpha_+(E)$ yields:

$$\alpha_+(^{20}\mathrm{F})-\alpha_-(^{20}\mathrm{Na}) \approx \frac{E}{2m_n Ac}\left[b-d_{\rm II}+\frac{3}{4\sqrt{14}}\frac{j_2}{m_n A}\Delta E_0\right] , \tag{4}$$

where $\Delta E_0=E_0(^{20}\mathrm{Na})-E_0(^{20}\mathrm{F})=5.84$ MeV, and j_2 and j_3 are assumed to be purely first-class interactions. Adding the two correlations yields:

$$\alpha_+(^{20}\mathrm{F})+\alpha_-(^{20}\mathrm{Na}) \approx \frac{E}{2m_n Ac}\left[1-d_{\rm I}-\frac{3}{4\sqrt{14}}\frac{j_2}{m_n A}\Delta' E_0\right] + \frac{E^2}{2m_n Ac}\left[\frac{3}{\sqrt{14}}\frac{j_2}{m_n A}-\frac{3}{\sqrt{35}}\frac{j_3}{m_n A}\right] , \tag{5}$$

where $\Delta' E_0=E_0(^{20}\mathrm{Na})+E_0(^{20}\mathrm{F})=17.66$ MeV. By invoking CVC,[1] the weak magnetism form factor can be deduced from the $M1$ gamma decay width of the analog γ transition in ^{20}Ne. Hence,

$$b=\left[\frac{6\Gamma_{m1}M^2}{\alpha E_\gamma^3}\right]^{1/2}=42.7\pm1.2 , \tag{6}$$

where Γ_{m1} is the $M1$ decay width,[6,7] M is the nuclear mass, $\alpha=\frac{1}{137}$, and E_γ is the γ transition energy between the analog state ($E_x=10.275$ MeV) and the first excited state ($E_x=1.663$ MeV). The form factor c can be determined from the beta decay ft value[6,8] by the relation,[3]

$$c=\left[\frac{6165}{ft}\right]^{1/2}=0.256\pm0.006 . \tag{7}$$

Therefore, for the $A=20$ system:

$$b/Ac=8.34\pm0.30 . \tag{8}$$

The task of measuring angular correlations to a fraction of a percent accuracy is a formidable one, especially if coupled with a short-life targetlike ^{20}Na. Hence, existing publications show large error bars, and some discrepancies exist. The beta-gamma angular correlation in ^{20}Na has been measured twice before. Dupuis-Rolin *et al.*[9,10] found

$$\alpha_-(E)=(-2.93\pm0.32)\times10^{-3}E +(0.78\pm0.40)\times10^{-4}E^2 ,$$

and Tribble *et al.*[11] reported

$$\alpha_-(E)=(-5.0\pm0.8)\times10^{-3}E+(2.9\pm0.8)\times10^{-4}E^2 .$$

The agreement between the two results is marginal. Furthermore, both experiments were performed in a very limited angular region, namely for $\theta_{\beta\text{-}\gamma}=90°$ and 180°.

In repeating this experiment over a wide angular region, we expected to obtain smaller statistical and systematic errors by using a sixteen-β-detector system of cylindrical symmetry. Detector-related asymmetries can be detected and eliminated more easily if data are taken over the full angular region. The ^{20}Na decay scheme is shown in Fig. 1. The ground state of ^{20}Na decays to the first excited state of ^{20}Ne ($E_x=1.633$ MeV), by an allowed Gamow-Teller transition which subsequently undergoes an $E2$ gamma ray emission. The end-point energy of the beta emission is 11.24 MeV. Additional ^{20}Na β^+ decays populate final states that subsequently α decay. We discuss our experimental procedure in Sec. II and the data analysis in Sec. III. Our results and the evaluation of $d_{\rm I}$, $d_{\rm II}$, and j_3, assuming CVC, are presented in Sec. IV.

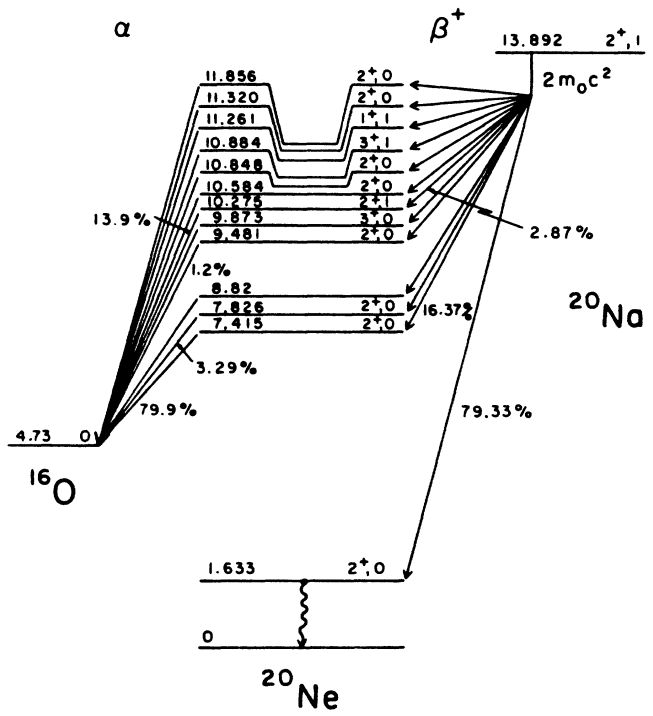

FIG. 1. Decay scheme of ^{20}Na and relevant levels of ^{20}Ne. The angular correlation of β^+ decay to the 1.633 MeV level of ^{20}Ne and the subsequent γ ray were measured in this study. Excitation energies and branching ratios are taken from Ref. 6.

II. EXPERIMENTAL PROCEDURE

The detector geometry is shown in Fig. 2. A 19 MeV proton beam from the Pittsburgh Tandem Van de Graaff Accelerator, incident on a neon gas target, was used to produce the ^{20}Na ($t_{1/2}$=445 ms) activity by the ^{20}Ne(p,n) ^{20}Na reaction. ^{20}F was produced by the ^{19}F(d,p)^{20}F reaction, using SF_6 gas and 4 MeV deuterons. The activated gasses were continuously transferred from a distant target cell into a source cell in the center of the correlation apparatus, through a thin capillary of 4.5 m length. The pressure of the gas in the irradiation and source cells (about 4 and 2 atm, respectively) and the length and diameter of the capillary (0.055 cm) were chosen to maximize the ^{20}Na activity in the source cell. The source cell was a plexiglass cylinder of 1.27 cm O.D., 2.5 cm height, and 0.079 cm wall thickness. θ_β was measured by 16 ΔE detectors in coincidence with a common E detector. Each ΔE detector was 40 mm high, 21 mm wide, and 1 mm thick, and made of Pilot-B plastic scintillators. They were coupled to 1 in. photomultiplier tubes (PM2982) through 11 cm long light pipes. The common E detector is a BC-400 plastic scintillator of annular shape and 236 mm O.D. It is 50 mm thick and 86 mm high, and optically coupled through the light pipe B to a 5 in Hamamatsu (R1584) photomultiplier tube. The E detector thickness (5 cm) was chosen to stop beta particles up to 12 MeV energy, in order to measure the total energy of beta particles.

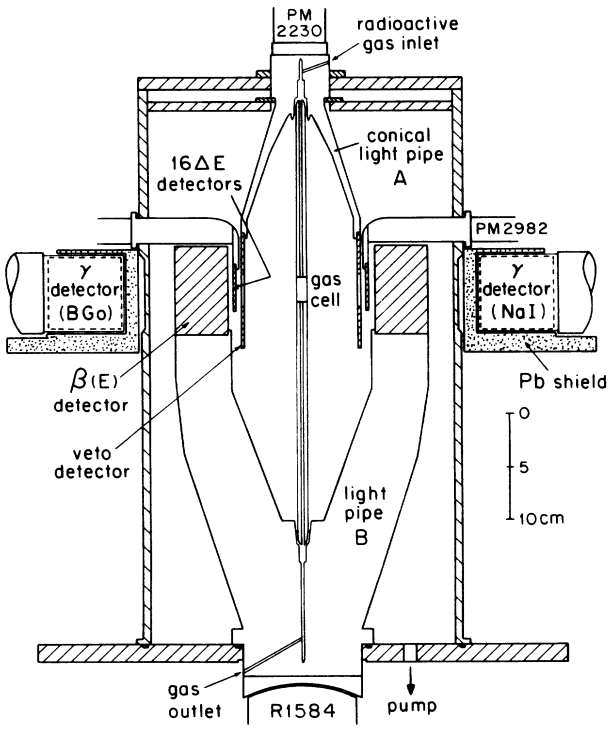

FIG. 2. Schematic view of the angular correlation apparatus. Apart from the γ detectors the apparatus has cylindrical symmetry.

The anticoincidence detector ("veto" detector in Fig. 2) defined the apertures. It was also made of Pilot-B scintillator and of cylindrical shape, 110 mm long, 110 mm O.D., and 2.5 mm thick. It had 16 carefully machined apertures to define the beta solid angle. Figure 3 shows a cross-sectional view of this aperture defining detector. If the gamma direction is defined as 0°, the nominal beta angles are θ_β=0°, 25°, 45°, 65°, 90°, 115°, 135°, 155°, and 180°, and their symmetric counterparts (360°$-\theta_\beta$) with respect to the 0°–180° direction. The two apertures at $\theta_{\beta\text{-}\gamma}$=0° and 180° were circles 20.0±0.1 mm in diameter, and all others were rectangles of width 13.7±0.1 mm and height 36.0±0.1 mm. The ΔE detectors were positioned right behind the apertures, aligned with them and the gas source cell. The output of the aperture defining detector was in anticoincidence with the (Δt = 10 ns) coincidence signal of E and ΔE detectors. This system accurately defined the opening angles by suppressing aperture edge scattering. It also eliminated most backscattered beta particles.

NaI and BGO detectors (7.62-cm diameter×7.62-cm length) were used for gamma detection. They were mounted outside the evacuated correlation apparatus along the 0°–180° axis. Both detectors were surrounded by lead shields, whose front face thickness was 1.5 cm. This resulted in a lowering of the 511 keV detection efficiency relative to the 1.663 MeV gamma ray by a factor of ~4. Furthermore, the shields reduced the background effects that could have been caused by gamma rays from decay in the feeding line. The correlation apparatus was kept at a rough vacuum of ~50 microns of Hg in order to minimize positron scattering in air.

Fast-slow electronics were used to record beta-gamma coincidences and beta and gamma energies. Data were fed through CAMAC electronics into a PDP11 computer via a microprogrammed branch driver (MBD) and recorded using the Los Alamos "Q" software package. Beta-gamma coincidence events were sorted into 32 two-dimensional histograms, 16 per gamma detector. A block diagram of the electronics is shown in Fig. 4. Outputs from the coincidence units served as gates for the analog

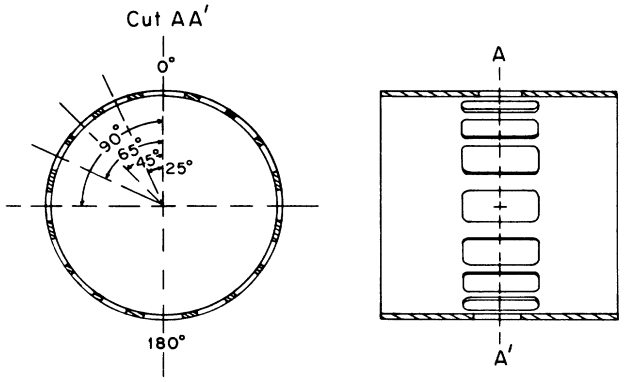

FIG. 3. Schematic diagram of the aperture-defining anticoincidence detector. The nominal β angles are shown for one quadrant.

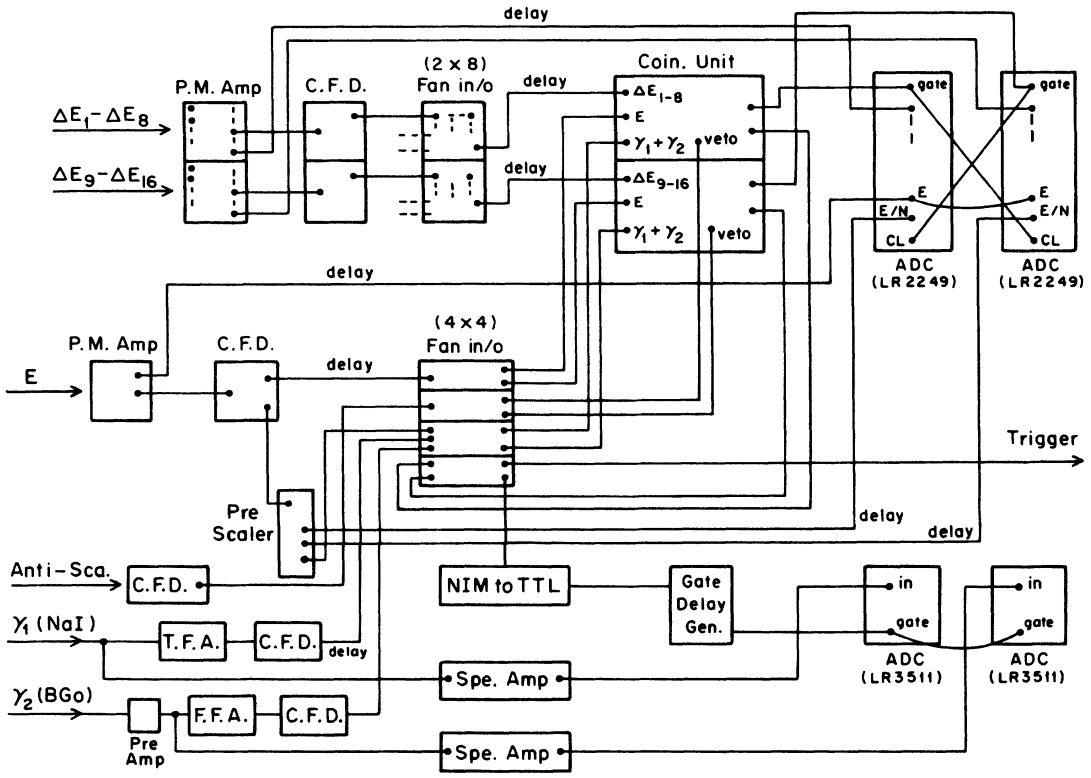

FIG. 4. The electronics setup. Boxes refer to photomultiplier amplifiers (P.M. Amp), timing filter amplifiers (T.F.A.), spectroscopy amplifiers (Spe. Amp), constant fraction discriminators (C.F.D.), logic fan in/out units (Fan in/o).

to digital converters, and their combined output was used as the event trigger. Two charge-sensitive ADC's (LR 2249W) read the ΔE and E signals, while two voltage-sensitive ADC's (LR 3511) recorded γ signals.

Instrumental alignment was monitored while gathering correlation data. This was accomplished by dropping the γ coincidence requirement, keeping only the $E,\Delta E$ coincidence, and the veto requirement. A prescaled logic signal (E/N) from the E detector (where N is the prescaler setting or the step-down factor) was used in place of a γ input to simulate isotropic γ signals. When ΔE pulses exceeded a minimum threshold, data flags were set according to the ΔE detector number. For an acceptable event, one and only one ΔE signal was permitted per event. The beta threshold was set at $\sim$0.5 MeV, while the γ energy thresholds were set above 0.511 MeV peak. The logic adopted for further event sorting can be displayed as follows:

$\gamma_{NaI}+\gamma_{BGO}$	E	E/N	Spectrum	Histogram no.
Yes	Yes	No	E-γ	1–16 (for BGO) 17–32 (for NaI)
No	Yes	Yes	E-ΔE	33–48

where Yes means pulse recorded and No means pulse not recorded.

The typical beam current on target was about 200 nA. Typical triple coincidences per sec were about 150 and 250 for the NaI and BGO detectors, respectively. Figure 5 shows a triple coincidence beta spectrum taken at $\theta_{\beta\text{-}\gamma}=90°$.

A. Data analysis and experimental results

All data analysis apart from the sorting mentioned above was performed off line. Coincidence gamma spectra for $\theta_{\beta\text{-}\gamma}=90°$ and 0° are compared in Fig. 6(a) and Fig. 6(b). For forward angle gamma spectra there is a significant background due to coincidence between positrons and continuum gammas from positron annihilation in flight. Therefore only correlation angles of 65° to 180° and their symmetric counterparts were analyzed. The coincidence gamma spectra of these larger angles showed nearly uniform background. This was checked by summing the gamma counts above the photo peak. Moreover in order to further reduce any correlation related to the annihilation in flight, only beta coincidence events within the FWHM of the 1.633 MeV gamma ray were considered in the analysis.

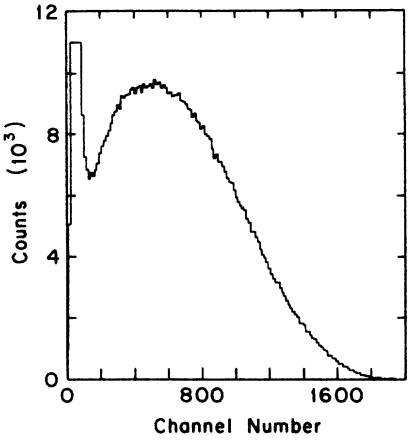

FIG. 5. Event spectra for β's in triple coincidence taken at the correlation angle $\theta_{\beta\text{-}\gamma}=90°$.

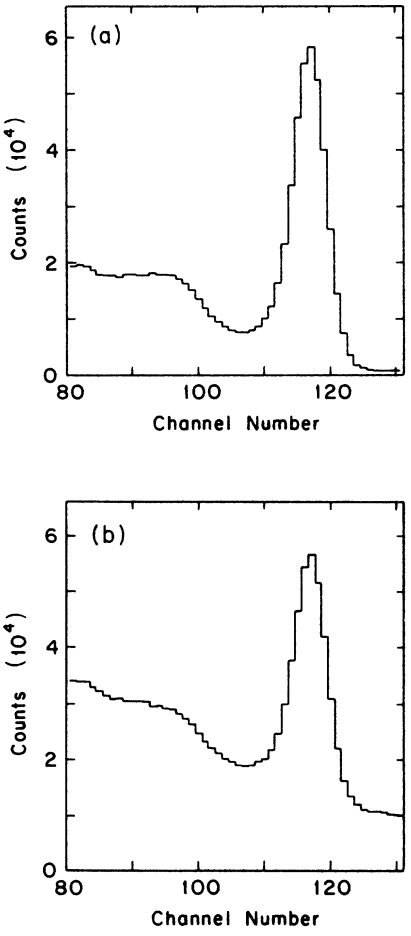

FIG. 6. Coincidence γ ray spectra (a) at $\theta_{\beta\text{-}\gamma}=90°$ and (b) at $\theta_{\beta\text{-}\gamma}=0°$. The energy of the γ ray peak is 1.633 MeV. The higher background seen at $\theta_{\beta\text{-}\gamma}=0°$ is due to the continuum from positron annihilation in flight. (The solid angle at 0° is 1.5 times less than that at 90°.)

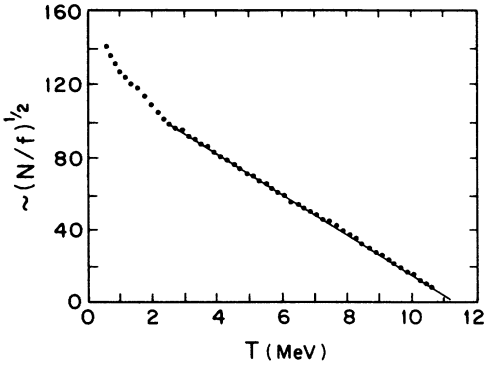

FIG. 7. Kurie plot of a typical β^+ spectrum corrected for detector resolution and backscattering of β's from the E scintillator. The data points are separated by about 200 keV and the statistical uncertainty associated with each point is of the order of the size of the point, or smaller.

Beta energy spectra were calibrated using Kurie plots. Figure 7 shows a typical Kurie plot for $\theta_{\beta\text{-}\gamma}=90°$, corrected for finite detector resolution, and backscattering from the E scintillator. An iterative summing procedure described by Freedman *et al.*[12] was performed to correct both effects mentioned above. The experimentally measured spectrum is related to the true spectrum by the equation:

$$M(E_0)=\int_0^{E_{\max}} N(E)L(E,E_0)dE$$
$$\approx\Sigma_i N(E_i)L(E_i,E_0)\Delta_i E\ , \tag{9}$$

where $M(E_0)$ are the observed counts at energy E_0, $N(E)$ denotes the actual counts at energy E, and $L(E,E_0)$ is the folding function. A Gaussian function with an energy-dependent backscattering tail was used as the folding function. The backscattering tail was determined from the calculations reported by Kuzminikh *et al.*[13] Using the normalized folding function, a simple iterative method was carried out to obtain $N(E)$, by matching the experimental spectrum $M(E_0)$ with that calculated from Eq. (9). The departure from linearity of the Kurie plot at low energy is due to background and a low energy β^+ line in true coincidence, which precludes using the very low energy data.

After calibrating each beta spectrum, the coincidence events per beta kinetic energy bin were extracted, for each correlation angle for kinetic energies ranging from 2.75 to 10.75 MeV in 0.5 MeV steps. Figure 8(a) shows the measured $\cos^2(\theta_{\beta\text{-}\gamma})$ asymmetry for the slice centered at a total energy of 6.26 MeV, after correction for the instrumental asymmetry. The measured instrumental asymmetry is shown in Fig. 8(b). It can be explained by a small 0.043 ± 0.006 mm displacement of the effective source axis from the geometrical axis of the apparatus. One can see that the effect of apparatus asymmetry is of different shape ($\cos\theta$) and small compared to the decay anisotropy. Similar fits were performed for each energy slice, and the asymmetry as a function of β^+ energy was extracted.

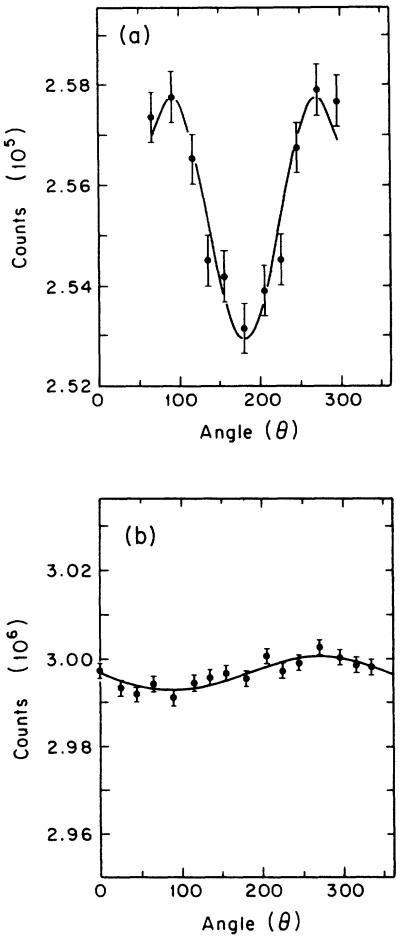

FIG. 8. (a) Measured anisotropy as a function of the correlation angle for the energy bin centered at total energy 6.26 MeV. (b) Measured instrumental asymmetry.

B. Geometrical and systematic corrections

Geometrical corrections must be applied in order to extract $\alpha_{\pm}(E)$ from the data. These corrections arise from (i) finite detector solid angle, (ii) finite source size, and (iii) displacement of the source from the geometrical center. The angular correlation $W(\theta_{\beta\text{-}\gamma})$ has to be integrated over the solid angle subtended by the gamma and beta detectors and over the volume of the source. This integration was carried out by Niedra[14] for the geometry of our angular correlation system. Due to the above effects the measured anisotropy is smaller (attenuated) than the actual decay anisotropy. The attenuation factor (κ) in the $\cos^2\theta_{\beta\text{-}\gamma}$ term can be defined as:

$$\kappa=\frac{\alpha_{\pm}(E)_{\text{actual}}}{\alpha_{\pm}(E)_{\text{measured}}} . \tag{10}$$

We computed $\kappa=1.33$ for the geometry of this experiment.

The $\cos^2(\theta_{\beta\text{-}\gamma})$ asymmetry arising from the displacement (δ) of the source from the geometrical center, with $\delta=0.043$ mm, is about 0.004% and is negligible. Other terms contributing to the $\cos^2(\theta_{\beta\text{-}\gamma})$ anisotropy are even smaller than the above value.

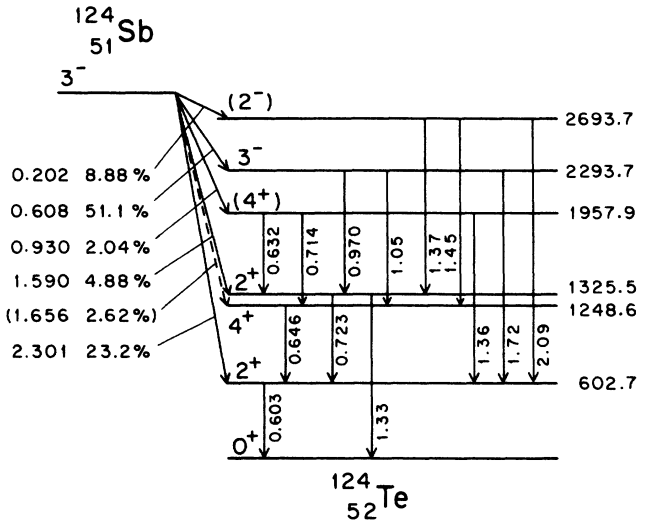

FIG. 9. Decay scheme of ^{124}Sb. Excitation energies, branching ratios, and beta endpoint energies are taken from Ref. 33.

The computed attenuation or "wash-out" [Eq. (10)] of the measured anisotropy was cross checked experimentally by measuring the large known[15,16] anisotropy of ^{124}Sb beta-gamma angular correlation. The relevant decay scheme of ^{124}Sb is shown in Fig. 9. The ^{124}Sb(3^-) ground-state decays to the first excited state (2^+) of ^{124}Te by a first forbidden β^- decay, with an end point energy of 2.301 MeV, followed by a γ-ray emission of 603 keV. This correlation has a measured maximum anisotropy of about 40% (Refs. 15 and 16); therefore it was one of the best ways to check the instrumental attenuation factor.

The ^{124}Sb source was obtained from California Isotope Products Laboratories. The activity was deposited on a 0.25 mil thick Aluminized mylar foil covered with a 2.5 mil Kapton protective foil, and then wrapped over a clear plexiglas (1.5 mm wall thickness) tube. The cylindrical diameter of the source material was 7.86 mm, and the active height was 25 mm. The above dimensions were chosen to match the effective size of the gas cell. (The computed κ for the geometry with the ^{124}Sb source is $\kappa=1.28$. The "measured" value was 1.30 ± 3 %.) The ^{124}Sb source was mounted in place of the gas cell. The NaI and BGO detectors were replaced by two high-purity Ge detectors in order to resolve the deexcitation gamma rays. A coincidence gamma spectrum is shown in Fig. 10 which includes the 0.603 MeV gamma ray.

The angular distribution of the β^- (2.301 MeV)$\rightarrow\gamma$ (0.603 MeV) correlation can be written as:[15]

$$W(\theta_{\beta\text{-}\gamma})=1+A_2(\mathcal{W})P_2(\cos\theta_{\beta\text{-}\gamma}) , \tag{11}$$

where

$$A_2(\mathcal{W})=\left[\frac{\mathcal{W}^2-1}{\mathcal{W}}\frac{R_3+e\mathcal{W}}{1+a\mathcal{W}+c\mathcal{W}^2+(b/\mathcal{W})}\right] . \tag{12}$$

$P_2(\cos\theta_{\beta\text{-}\gamma})$ is the second Legendre polynomial, and $\mathcal{W}$ is the total energy of electrons in units of mc^2. The

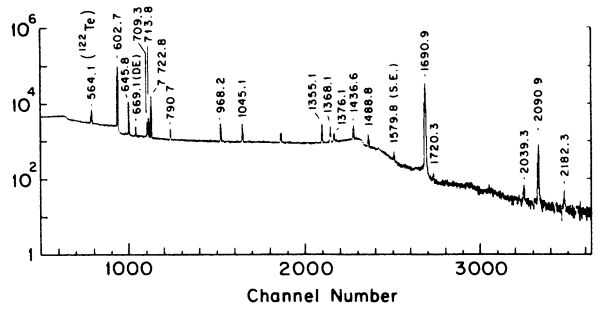

FIG. 10. The deexcitation gamma ray spectrum following ^{124}Sb β^- decay in coincidence with β's.

coefficients R_3, e, a, b, and c are functions of the matrix element parameter[15,17] which can contribute to a first forbidden β transition with $\Delta J = \pm 1$, yes. Figure 11 shows the measured anisotropy as a function of the correlation angle for the energy bin centered at $E = 2.5$ MeV. Since for electron decay there is no annihilation in flight continuum to deal with, correlation data over the full angular region were used to deduce $A_2(\mathcal{W})$. Assuming the calculated values for the above matrix element parameters from Refs. 15 and 17, $A_2(\mathcal{W})$ was fitted, according to Eq. (12), to obtain the attenuation factor (κ) defined in Eq. (10). The least squares fits shown in Figs. 11 and 12 yielded $\kappa = 1.30 \pm 0.04$. Hence, within the experimental errors, the measured attenuation factor agreed with the computed value; or conversely, our new measurement confirms the earlier data to $\pm 3\%$.

In ^{124}Sb there is an inner beta group with an end point energy of 1.59 MeV. Therefore, at beta energies less than 1.59 MeV contributions from the $\beta \rightarrow$(0.723 MeV γ)$\rightarrow$0.603 MeV γ cascade were also included. Due to the finite energy resolution of the E detector (20% at 3 MeV), this cascade is not fully resolved for β's up to 2 MeV. As the contaminant β-γ correlation has less asymmetry than the primary one, the measured asymmetries

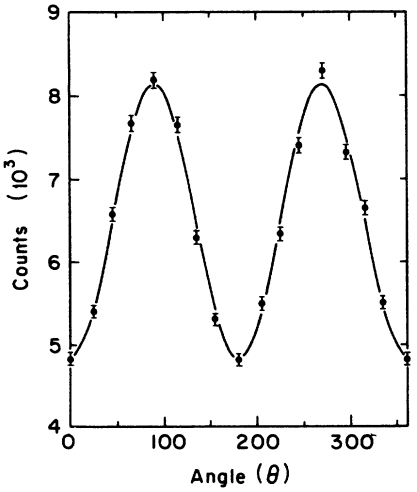

FIG. 11. Measured asymmetry as a function of the correlation angle for the slice centered at $E = 2.5$ MeV. The solid line represents the least-square fit of the type $W(\theta_{\beta\text{-}\gamma}) = 1 + A_2(\mathcal{W})P_2(\cos\theta_{\beta\text{-}\gamma})$ where $A_2(\mathcal{W})$ was extracted for each energy slice.

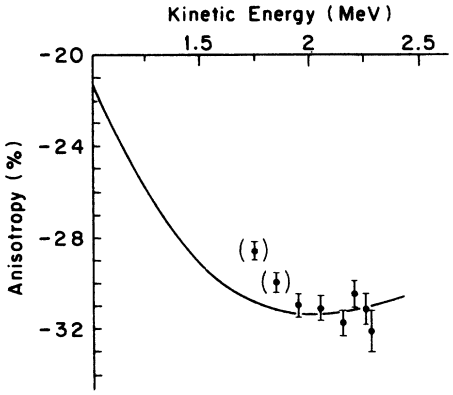

FIG. 12. Energy dependence of the anisotropy factor $A_2(\mathcal{W})$ of the 2.301 MeV $\beta \rightarrow$0.603 MeV γ directional correlation. The solid line represents the least square fit performed to check the attenuation factor defined in the text.

near 1.59 MeV ($W = 4.12$) are attenuated. The questionable points are shown in parentheses in Fig. 12, and were not included in the fit that determined κ.

We have estimated the effect of other possible energy dependent systematic effects on the deduced asymmetries, such as multiple scattering from the source wall and positron annihilation in flight. Multiple scattering effects were found to be small and negligible for beta energies greater than 3 MeV. The annihilation in flight continuum does not seriously affect larger correlation angles. However, the possibility that a positron can annihilate in flight in the E scintillator does have a systematic effect on the E dependence of the measured asymmetry. This can be viewed in the following way. If an 11 MeV beta particle loses only 4 MeV in the E detector and then annihilates it will be recorded as a 4 MeV particle, but the observed asymmetry belongs to the 11 MeV particle. Therefore, for positrons the asymmetry at low energies is "measured" a little higher than what it should be. The effect decreases as the measured energy increases. In other words, a small fraction of the measured anisotropy at a

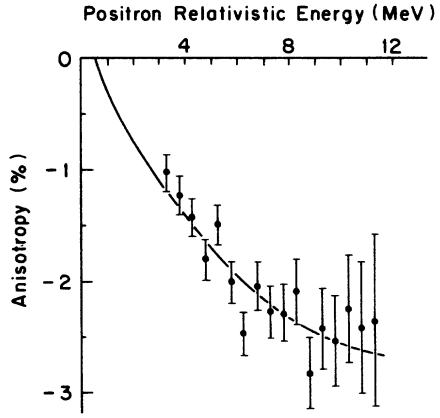

FIG. 13. Percentage anisotropy $[\alpha_-(E)(p/E)^2 \times 10^{+2}]$ as a function of the total (relativistic) β^+ energy for β^+-γ correlation in ^{20}Na, with all corrections included. The solid line represents the third (two parameter) least square fit given in Table II.

TABLE I. Results for the anisotropy $[\alpha_-(E)(p/E)^2]$ in ^{20}Na as a function of total positron energy.

E (MeV)	$[\alpha_-(E)(p/E)^2]\times 10^2$
3.26	−1.078±0.179
3.76	−1.274±0.178
4.26	−1.471±0.176
4.76	−1.814±0.180
5.26	−1.532±0.186
5.76	−2.011±0.192
6.26	−2.473±0.203
6.76	−2.046±0.222
7.26	−2.269±0.237
7.76	−2.282±0.259
8.26	−2.089±0.291
8.76	−2.824±0.324
9.26	−2.421±0.368
9.76	−2.535±0.409
10.26	−2.245±0.482
10.76	−2.418±0.591
11.26	−2.357±0.779

given (low) energy really belongs to some high energy positron that annihilated having deposited only part of its full energy. Using Bethe's[18] formula for the probability of positron annihilation in flight, and taking care of the beta spectrum shape by allowing for the fact that all beta energies are not equally probable, we made a systematic correction, although it was small compared with the uncertainty associated with each data point.

After correcting for all the effects mentioned above, the anisotropy for ^{20}Na as a function of relativistic positron energy is shown in Fig. 13 and tabulated in Table I. Allowing for a nonzero intercept (A) at zero positron kinetic energy the anisotropy $\alpha_\pm(E)$ can be written as

$$\alpha_\pm(E)=A_0+(B_\pm E+CE^2)(p/E)^2 . \quad (13)$$

Results of three different least squares fits are given in Table II. As expected when all three parameters (A_0, B_-, and C) are allowed to vary, the uncertainties in the

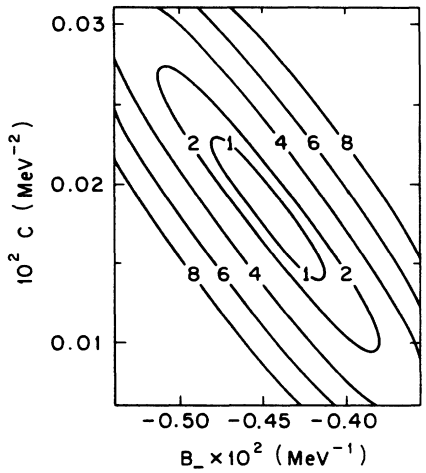

FIG. 14. The confidence regions (x^2 contours) for parameters B_- and C of the two parameter fit of Fig. 12.

B_- and C coefficients are large. The A_0 (intercept) coefficient is fully consistent with zero in the three parameter fit. This supports our assumption that in design and analysis we have taken into account all systematic contributions that are pertinent in extracting the asymmetry. When the coefficient A_0 was fixed at (-10.3×10^{-4}), the uncertainties of B_- and C reduced significantly, as seen in the second least square fit. The results of the third least square fit given in Table II were obtained by assuming $A_0=0.0$ and allowing only B_- and C to vary. This two-parameter fit is shown in Fig. 13. The confidence regions (error contours) for parameters B_- and C are shown in Fig. 14. From the eccentricity of the contours it is easy to see that both parameters are highly correlated. A small change in parameter B_- is associated with a large variation in C, and this is reflected in the relatively large errors associated with C and B_-.

We also measured the β-γ correlation for the ^{20}F→^{20}Ne mirror transition, using the same experimental setup and procedure as above. Since the asymmetry had been measured repeatedly, and is very small[10,19,20]

TABLE II. Results for the least squares fits of the ^{20}Na and ^{20}F correlation data to a function $\alpha_-(E)=A+(B_-E+CE^2)(p/E)^2$, and $\alpha_+(E)=A+(B_+E)(p/E)^2$, respectively. p is beta momentum and E is the total relativistic beta energy.

	^{20}Na		
Fit	A_0 (10^{-4})	B_- (10^{-3} MeV^{-1})	C (10^{-4} MeV^{-2})
Three parameter	−10.3±46.1	−4.35±1.56	1.90±1.22
Fixed	−10.3	−4.35±0.29	1.90±0.40
Two parameter	0.00	−4.45±0.31	1.87±0.42
	^{20}F		
		B_+ (10^{-3} MeV^{-1})	C (10^{-4} MeV^{-2})
Two parameter	+6.25±13.00	+0.60±0.40	0.0
One parameter	0.0	+0.80±0.20	0.0

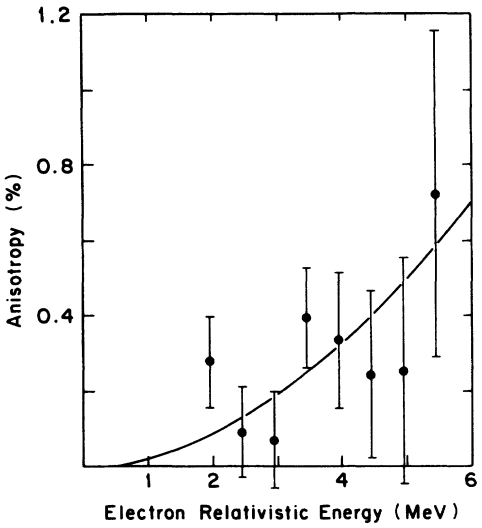

FIG. 15. Percentage anisotropy $[\alpha_+(E)(p/E)^2\times 10^{+2}]$ as a function of the total (relativistic) β^- energy for the β^--γ correlation in ^{20}F. The solid line represents the two parameter fit performed for the correlation data to deduce B_+, by using the value C obtained from the ^{20}Na correlation.

relative to the ^{20}Na correlation, our primary motivation was to catch any systematic or instrumental asymmetry which had not been seen in the ^{20}Na analysis. The data analysis was the same as described above except for the fact that there was no annihilation in flight correction for the electrons.

The corrected anisotropy for ^{20}F as a function of total relativistic electron energy is shown in Fig. 15. Because of the low end point energy for the ^{20}F decay, it is difficult to deduce the quadratic term from the ^{20}F data to a reasonable accuracy. For this reason authors of previously published work[10,19,20] neglect C completely and present their best value for B_+ as a result of a linear least squares fit to the data. We feel that this procedure is inaccurate, as will be discussed in Sec. IV. Nevertheless in order to compare our data with published data, a linear least squares fit was performed with and without the zero intercept. Results are given in Table II under ^{20}F.

IV. DISCUSSION AND CONCLUSIONS

We suggest that the results of the two-parameter fit give the best estimates of the B_- and C coefficients and their uncertainties, since we cannot find any reason to believe that the intercept A is other than zero. A summary of the results for the ^{20}Na β-γ correlation is given in Table III. In addition the table contains the most recent results for the linear coefficient in the ^{20}F (β-γ) angular correlation (Refs. 10, 19, and 20), assuming a zero quadratic term. Our results for ^{20}Na are in good agreement with the measurement quoted in Ref. 11. In Ref. 9 Dupuis-Rolin *et al.* reported $\alpha_-(E)=(-4.0\pm 0.7)\times 10^{-3}E+(1.3\pm 0.9)\times 10^{-4}E^2$, but in Ref. 10 after correcting for an instrumental asymmetry, the relation became

$$\alpha_-(E)=(-2.93\pm 0.32)\times 10^{-3}E$$
$$+(0.78\pm 0.40)\times 10^{-4}E^2 .$$

Our result is in poor agreement with Ref. 10 (after corrections). Using the data from Ref. 10, Tribble *et al.*[11] pointed out that they were not able to reproduce the uncertainties quoted for the correlation coefficients. They independently derived the uncertainties for the linear and quadratic coefficients for Ref. 10 as 0.5×10^{-3} MeV^{-1} and 0.6×10^{-4} MeV^{-2}, respectively. Our new results for the ^{20}Na correlation have uncertainties about factor of two better in the linear coefficient than the best published errors.[11]

According to Eq. (2), the sign of b changes between ^{20}Na(β^+) and ^{20}F(β^-) decays, so the linear coefficients in E are different for ^{20}Na and ^{20}F decays. As a matter of fact, for ^{20}F(β^-) decay b is positive, hence its contribution to the correlation is masked by d_1 which has a minus sign. For ^{20}Na, the sign of b is negative, therefore it will add to d_1 and enhance the asymmetry.

Because of the low end point energy for the ^{20}F decay, it is difficult to derive the quadratic term directly from the data. But, if we assume that j_2 and j_3 have negligible second class contributions, the quadratic coefficient (C) should be the same for ^{20}Na and ^{20}F. Therefore one can use the value of C obtained from ^{20}Na angular correlation to deduce a much more reliable value for B_+. The earlier neglect of C in deducing B_+ is misleading, since the

TABLE III. β-γ angular correlation measurements in $A=20$.

Parent nucleus	Ref.	B_- (10^{-3} MeV^{-1})	C (10^{-4} MeV^{-2})
^{20}Na[a]	10	-2.93 ± 0.5	0.78 ± 0.6
^{20}Na	11	-5.0 ± 0.8	2.9 ± 0.8
^{20}Na	present	-4.45 ± 0.31	1.87 ± 0.42
^{20}Na	weighted average	-4.12 ± 0.25	1.74 ± 0.32
		B_+ (10^{-3} MeV^{-1})	
^{20}F	present	$+0.60\pm 0.40$	
^{20}F	10	$+0.41\pm 0.18$	
^{20}F	19	$+0.5\pm 0.7$	
^{20}F	20	$+0.9\pm 0.7$	

[a]The uncertainties quoted here are taken from the reevaluation of the Ref. 10 data by Tribble *et al.* (Ref. 11).

TABLE IV. Results of the reevaluation of linear coefficient (B_+) in ^{20}F asymmetry data using measured value of C [$(1.87\pm0.42)\times10^{-4}$ MeV^{-2}] from ^{20}Na asymmetry. Reference 20 data were not published. The errors were obtained folding in the lower and upper experimental limits for C.

Ref.	B_+ (10^{-3} MeV^{-1})
Present	0.08±0.16
10	0.06±0.17
19	−0.07±0.16

contribution from C is important for the ^{20}F anisotropy. In fact at higher β^- energies, C dominates over B_+. For example, if $C=1.87\times10^{-4}$ MeV^{-2} (taken from ^{20}Na asymmetry); then at $E=5$ MeV, $CE^2=0.5\%$, which gives almost all the observed anisotropy of ^{20}F.

As seen from Table III our linear fit for the ^{20}F correlation agrees with the equivalent earlier determinations. However, due to the fact discussed above, this value for B_+ should *not* be used to extract induced currents. Therefore a least squares fit was performed for the data shown in Fig. 15, by using C obtained from the ^{20}Na correlation. The extracted value for B_+ was much smaller than the value obtained by neglecting C, and is given in Table IV. The errors quoted were obtained by also fitting the data with the lower limit for C (1.45×10^{-4} MeV^{-2}), and the upper limit for C (2.29×10^{-4} MeV^{-2}), respectively. Previously published data were reanalyzed in the same manner (using our value for C) to obtain more accurate estimates for B_+. Results are given in Table IV.

A. Evaluation of d_{II} and d_I

As stated in the introduction, d_{II} and d_I can be evaluated by combining the linear coefficients (B) in E of $\alpha_\pm(E)$. However, as can be seen from Eq. (4), one cannot neglect the contribution of j_2 in evaluating d_{II} since the end point energies differ considerably for ^{20}Na and ^{20}F decays. d_I and d_{II} were first evaluated using present results alone. In addition, they were evaluated using the average of B_- and B_+. j_2 was taken as -3.89×10^4, according to the calculations of Calaprice *et al.*,[21] and the phase correction reported in Ref. 19.

The results for d_I/Ac, and d_{II}/Ac are given in Table V. In the first column, they are presented assuming no uncertainty for the computed second forbidden correction (j_2), and in the second column, assuming 100% uncertainty in j_2. As pointed out earlier, because of the uncertainty in j_2, d_I and d_{II} retain some ambiguity. Assuming that j_2 has been calculated accurately, our data suggest a small contribution from second-class currents. If other existing data are included for a weighted average, the error becomes slightly smaller, and the mean value for d_{II}/Ac is closer to zero suggesting a vanishing contribution of d_{II}, as shown in Table V. If one assumes a 100% uncertainty in j_2, d_{II}/Ac is consistent with zero, in both cases. In any case, one can conclude that contributions from second class currents play at best a minor

TABLE V. Deduced values for d_I/Ac and d_{II}/Ac using B_- and B_+.

	From present results: No uncertainty in J_2	From present results: 100% uncertainty in J_2
d_{II}/Ac	−1.1±0.7	−1.1±1.2
d_I/Ac	+11.3±0.7	+11.3±3.0
	From weighted average	
d_{II}/Ac	−0.4±0.6	−0.4±1.1
d_I/Ac	+10.6±0.6	+10.6±2.9

role in the beta-gamma angular correlation in mass 20. Recent measurements[22,23,24] of β-α correlation for $A=8$ and polarization-beta correlations in the super-allowed $A=12$ and 19 decays (for $A=12$ see Refs. 25, 26, and 27, and for $A=19$ see Refs. 28 and 29) suggest that second-class currents may be absent. It is worth noting that the d_{II}/Ac values obtained from the experiments on mass 20 are in excellent agreement with those obtained from the mass 8 system. They all are essentially consistent with $d_{II}/Ac=0$, although there is a suggestion of a small negative value. Given our new data, the error bars for mass 20 have become comparable to those for mass 8.

The first-class induced tensor interaction (d_I) disagrees significantly with the theoretical calculation of Calaprice *et al.*,[21] where they found $d_I/Ac=4.0$. As pointed out previously[30,31] meson exchange effects could be important for the axial vector form factors, especially since d_I arises from the time part of the axial current.[32] Since meson exchange and higher-order many-body effects are neglected completely in the impulse approximation treatment, the accuracy of its predictions is uncertain. Therefore a large exchange contribution could change the impulse approximation prediction for the first class induced tensor interaction. Previous measurements for d_I/Ac for mass 8 are very uncertain, whereas our new results determine this value to better than 30%, perhaps as well as ±6% (depending on the reliance placed on j_2).

B. Evaluation of j_3

From the quadratic term coefficient C, j_3 can be evaluated, assuming j_2 is known from wave function calculations.[21] This determination can then be compared with the calculated value of j_3. From Eq. (2):

$$C=\frac{1}{4mM_nAc}\left[\frac{3}{\sqrt{14}}\frac{j_2}{m_nA}-\frac{3}{\sqrt{35}}\frac{j_3}{m_nA}\right], \quad (14)$$

with $C=(1.87\pm0.42)\times10^{-4}$ MeV^{-2}, which is similar to the average of previously measured values, although it has a much smaller error; and using $j_2=-3.89\times10^4$ we obtain for j_3

$$j_3=-(19.5\pm3.0)\times10^4 .$$

This is about twice the value computed by Calaprice ($j_3=-7.75\times10^4$), although it must be mentioned that

the uncertainty given is only our experimental uncertainty and does not include that of j_2. The lowest experimental limit for j_3 is about a factor of 2 larger than the wave-function prediction for j_3.

The existence of new experimental results with smaller errors, and consistent with the lower mass data, should give impetus to better theoretical calculations for the nuclear matrix elements j_2, j_3, and d_1 entering the calculations. The disagreement of the theoretical and empirical j_3 result certainly indicates a need for a more sophisticated theoretical analysis.

ACKNOWLEDGMENTS

The authors are indebted to Dr. Ana M. Hernandez for constructing much of the correlation apparatus in the early phases of this study. Thanks are due to Dr. J. M. Niedra for having computed the geometrical corrections for the finite detector geometries mentioned in the text. This work was supported by the National Science Foundation.

[1]M. Gell-Mann, Phys. Rev. **111**, 362 (1958); R. P. Feynman and Gell-Mann, *ibid.* **109**, 193 (1958).
[2]S. Weinberg, Phys. Rev. **112**, 1375 (1958).
[3]B. R. Holstein, Rev. Mod. Phys. **46**, 789 (1974); Erratum, *ibid.* **49**, 247 (1977); private communication.
[4]S. Weinberg, Phys. Rev. Lett. **19**, 1264 (1967).
[5]S. Weinberg, Phys. Today **30**, 42 (1977).
[6]F. Ajzenberg-Selove, Nucl. Phys. **A475**, 117 (1987).
[7]L. K. Fifield, F. P. Calaprice, C. H. Zimmerman, M. J. Hurst, A. Pakkanen, T. J. M. Symons, F. Watt, and K. W. Allen, Nucl. Phys. **A288**, 57 (1977).
[8]D. E. Alburger and F. P. Calaprice, Phys. Rev. C **12**, 1690 (1975).
[9]N. Rolin, J. P. Deutsch, D. Favart, M. Lebrun, and R. Prieels, Phys. Lett. **70B**, 23 (1977). N. Rolin, Ph.D. thesis, University of Louvain, 1979 (unpublished).
[10]N. Dupuis-Rolin, J. P. Deutsch, D. Favart, and R. Prieels, Phys. Lett. **79B**, 359 (1978).
[11]R. E. Tribble, D. P. May, and D. M. Tanner, Phys. Rev. C **23**, 2245 (1981).
[12]M. S. Freedman, T. B. Novey, F. T. Porter, and F. Wagner, Jr., Rev. Sci. Instrum. **27**, 716 (1956).
[13]V. A. Kuzminikh and S. A. Vorobiev, Nucl. Instrum. Methods **129**, 561 (1975).
[14]J. Niedra, private communication (unpublished).
[15]R. M. Steffen, Phys. Rev. Lett. **4**, 290 (1960).
[16]S. K. Mitra, Nucl. Phys. **47**, 293 (1963).
[17]Tsuneyuki Kotani, Phys. Rev. **114**, 795 (1959).
[18]H. A. Bethe, Proc. R. Soc. London, Sect. A **150**, 129 (1935).
[19]R. E. Tribble and D. P. May, Phys. Rev. C **18**, 2704 (1978).
[20]R. D. McKeown, F. P. Calaprice, and D. E. Alburger (unpublished).
[21]F. P. Calaprice, W. Chung, B. H. Wildenthal, Phys. Rev. C **15**, 2178 (1977).
[22]R. E. Tribble and G. T. Garvey, Phys. Rev. C **12**, 967 (1975).
[23]A. M. Nathan, G. T. Garvey, P. Paul, and E. K. Warburton, Phys. Rev. Lett. **35**, 1137 (1975); **49**, 1056(E) (1982).
[24]R. D. McKeown, G. T. Garvey, and C. A. Gagliardi, Phys. Rev. C **22**, 738 (1980).
[25]H. Brändle, L. Grenacs, J. Lang, L. Ph. Roesch, V. L. Telegdi, P. Truttmann, A. Weiss, and A. Zehnder, Phys. Rev. Lett. **40**, 306 (1978); **41**, 299 (1978).
[26]P. Lebrun, Ph. Descheppor, L. Grenacs, J. Lehmann, C. Leroy, L. Palffy, A. Possoz, and A. Maio, Phys. Rev. Lett. **40**, 302 (1978).
[27]Y. Masuda, T. Minamisono, Y. Nojiri, and K. Sugimoto, Phys. Rev. Lett. **43**, 1083 (1979).
[28]W. E. Kleppinger, F. P. Calaprice, and D. Mueller, Bull. Am. Phys. Soc. **23**, 603 (1978).
[29]D. Schrieber, F. P. Calaprice, M. Dewey, A. Hallin, W. E. Kleppinger, D. Mueller, and M. Schneider, Bull. Am. Phys. Soc. **24**, 51 (1979).
[30]J. Delorme and M. Rho, Phys. Lett. **34B**, 238 (1971).
[31]K. Kubodera, J. Delorme, and M. Rho, Nucl. Phys. **B66**, 253 (1973).
[32]K. Kubodera, J. Delorme, and M. Rho, Phys. Rev. Lett. **40**, 755 (1978).
[33]T. Tamura, K. Miyano, and S. Ohya, Nucl. Data Sheets **41**, 413 (1984).